Acta Materialia 208 (2021) 116708

Contents lists available at ScienceDirect

Acta Materialia

journal homepage: www.elsevier.com/locate/actamat

Full length article

# Ultralow-current magnetization switching in nearly compensated synthetic antiferromagnetic frames using sandwiched spin sources

Seungmo Yang[a,1], Tae-Seong Ju[a,b,1], Jeongwoo Seo[b], Kyoung-Woong Moon[a], Changsoo Kim[a], Hyun-Joong Kim[a], Jeonghun Shin[b], JungYup Yang[c], Chanyong Hwang[a,*], Jinpyo Hong[b,*]

[a] Quantum Spin Team, Korea Research Institute of Standards and Science, Daejeon, 34113, Republic of Korea
[b] Research Institute of Convergence of Basic Science, Novel Functional Materials and Device Laboratory, Department of Physics, Hanyang University, Seoul, 04763, Republic of Korea
[c] Department of Physics, Kunsan National University, Gunsan, 54150, Republic of Korea

ARTICLE INFO

*Article history:*
Received 28 October 2020
Revised 21 December 2020
Accepted 28 January 2021
Available online 2 February 2021

ABSTRACT

Spin–orbit torque (SOT)-induced magnetization switching via electric currents in large spin–orbit-coupled heavy metal (HM)/ferromagnetic (FM) frames is one of the most reliable approaches to achieve increased performances in various spintronic applications. However, its widespread utilization is still challenging owing to the inherent requirement of a high electric current density for efficient magnetization switching. In this paper, we introduce a sandwiched synthetic antiferromagnetic (S-SyAF) frame, comprising CoFeB (FM)/W (HM)/CoFeB (FM) stacks, whose operation is mediated by the Ruderman–Kittel–Kasuya–Yosida interaction. The middle HM layer serves as a spin current source for the top and bottom FM layers simultaneously. In addition, the S-SyAF frame contributes to a substantial reduction in the net magnetization, which ensures a considerably increased SOT switching efficiency; further, the switching current was almost 10 times smaller than that in a conventional HM/FM frame. Thus, we believe that these experimental findings will provide a new avenue for designing future spintronic devices.



## 1. Introduction

In recent years, current-induced magnetization switching based on spin–orbit torque (SOT) has emerged as a promising alternative for use in spintronic applications [1-7]. Extensive studies have been performed to increase the SOT switching efficiency, and this is because SOT-driven magnetization switching has been expected to provide numerous advantages with regard to fabricating representative spin-orbit torque magnetic random-access memories. Particularly, such memories exhibit considerable advantages such as a low switching current density, fast dynamics, and absence of switching disturbance arising from separate read and write paths [8,9]. Thus, the achievement of a high SOT switching efficiency is important for various SOT-related spintronic applications. To ensure such characteristics, one promising approach is to specifically engineer the heavy metal (HM) layer in HM/ferromagnetic (FM) stacks to optimize the spin Hall angle (SHA), which reflects the charge-to-spin current conversion efficiency [10-13]. Zhang et al. reported a concept entailing spin transparency at the FM/HM interfaces, which augmented the amount of spin current injected to the FM layer [10]. Another approach is to use synthetic antiferromagnetic (SyAF) [14-17] or ferrimagnetic systems [18-20] owing to the reduced magnetization caused by antiferromagnetically coupled spins in both frames. The reduced magnetization implies a decrease in the angular momentum inherently necessary for magnetization switching.

A representative scheme of SOT-induced magnetization switching upon the application of electric current is shown in Fig. 1(a), where the electric current ($J_e$) enables the generation of spin current in the HM layer through the spin Hall effect (SHE), followed by the injection of this current into the FM layer. The injected spin current exerts a torque on the magnetization of the FM layer through the transfer of angular momentum, and this torque is referred to as the SOT [1]. Under an external magnetic field in the $x$-axis direction ($H_x$), parallel to the electrical current direction (the

* Corresponding authors.
*E-mail addresses:* cyhwang@kriss.re.kr (C. Hwang), jphong@hanyang.ac.kr (J. Hong).
[1] These authors contributed equally to this study

https://doi.org/10.1016/j.actamat.2021.116708

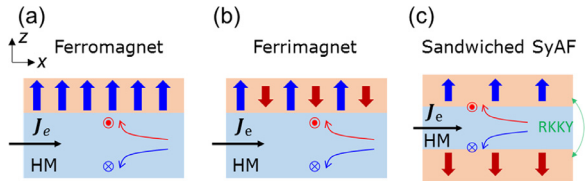


**Fig. 1. Basic schematics for the experimental concepts and conventional SOT frames.** Representative heterostructures of the (a) normal HM/FM and (b) HM/ferrimagnet frames. The red and blue arrows indicate the directions of the spin currents generated by the SHE; the spin direction of the spin current is described. (c) S-SyAF frame containing the sandwiched spin source layer, where both FM layers are chosen to be antiferromagnetically coupled by the RKKY interaction, thereby enabling injection of both spin currents (up and down) into the top and bottom FM layers, simultaneously.

coordinates are defined in Fig. 1), the SOT switches the magnetization of the FM layer toward the $\pm z$ axis, depending on the current direction with respect to the $H_x$ direction [2].

To quantify the SOT efficiency ($\chi$), defined as $H_{\text{eff}}/J_e$, where $H_{\text{eff}}$ is the effective magnetic field generated by the SOT and $J_e$ is the current density flowing through the HM layer, $\chi$ can be expressed by the following material parameters [21,22]

$$\chi = \frac{\pi}{2}\frac{\hbar\theta_{\text{SHE}}}{2e\mu_0 M_S t_{\text{FM}}}, \quad (1)$$

where $\hbar$ is the reduced Planck's constant, $\theta_{\text{SHE}}$ is the SHA, $\mu_0$ is the vacuum permeability, $e$ is the elementary charge, $M_S$ is the saturation magnetization, and $t_{\text{FM}}$ is the thickness of the FM layer. Eq. (1) reflects the occurrence of a larger $\chi$ in a system with a lower magnetization. For example, the SyAF systems adjacent to the HM layer led to an enhancement in $\chi$ owing to reduced magnetization. In addition, the ferrimagnetic systems shown in Fig. 1(b) also exhibited an increase in $\chi$ by the manipulation of operating temperatures, where higher enhancements in $\chi$ appeared at magnetization compensation temperatures [18-20]. However, the extensive utilization of the latter has the disadvantage of introducing temperature as a control parameter, which is not a desirable approach for the development of spintronic devices. In addition, conventional HM/FM, SyAF, and ferrimagnetic systems geometrically employed only 50% of the spin currents (up or down) generated by the SHE for magnetization switching, as shown in Fig. 1(a) and (b).

In this paper, we introduce a sandwiched SyAF system (S-SyAF) that includes a CoFeB (FM)/W (HM)/CoFeB (FM) stack as a crucial geometry. Although previous reports [23-25] also addressed the interesting results of SOT behavior by utilizing the FM/HM/FM layers, the sandwiched spin-source concept has not been introduced yet. Our geometry enabled the middle HM layer to generate opposite spin currents (up and down) directed toward the top and bottom FM layers upon the application of electric current with the Ruderman-Kittel-Kasuya-Yosida (RKKY) interaction, as illustrated in Fig. 1(c) [26-28]. A suitable manipulation of the RKKY interaction implements distinct antiferromagnetic coupling between the two FM layers, and thus facilitates efficient reduction of the total magnetization. Thus, the S-SyAF frame coupled with the RKKY interaction presents the possibility of the generation of two opposite spins owing to the SHE in the middle HM layer (red and blue arrows in Fig. 1(c)), which affects the top and bottom FM layers simultaneously. The identical magnitudes of the individual SOTs can separately affect each FM layer, which implies that the total magnitude of the SOT on the overall system is twice that in Fig. 1(a). This double SOT characteristic can enable outstanding SOT switching characteristics, together with a reduction in magnetization arising from the antiferromagnetic RKKY interaction, which favors the antiparallel magnetization alignment of the top and bottom FM layers. The SOT switching occurs between "up/down" and "down/up"

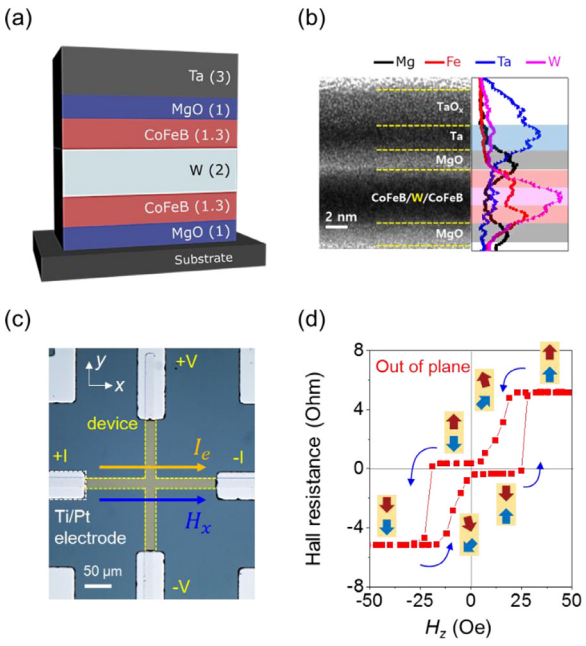


**Fig. 2. Structural and magnetic characteristics of the S-SyAF frame.** (a) Stack of MgO (1 nm)/CoFeB (1.3 nm)/W (2 nm)/CoFeB (1.3 nm)/MgO (1 nm)/Ta (3 nm) for the S-SyAF frame. (b) Representative cross-sectional HRTEM image of the S-SyAF frame and corresponding EDS line scan, which confirms the presence of individual FM layers well separated by the HM layer. (c) Optical image of the Hall bar structure, where Ti (3 nm)/Pt (50 nm) was used. (d) Typical out-of-plane magnetic hysteresis loops for S-SyAF with specific magnetization configurations (red and blue arrows) of the two FM layers.

configurations, depending on the electric current direction with respect to $H_x$. An example of the top/bottom CoFeB magnetization directions (up/down) is shown in Fig. 1(c) to clarify the detailed magnetization configurations of the top and bottom CoFeB layers.

## 2. Experimental methods

S-SyAF stacks of MgO (1 nm)/CoFeB (1.3 nm)/W (2 nm)/CoFeB (1.3 nm)/MgO (1 nm)/Ta (3 nm) on a $SiO_2$ substrate were fabricated (Fig. 2(a)). All layers were deposited by magnetron sputtering at a base pressure of $7 \times 10^{-8}$ Torr, followed by post-annealing at 350°C for 30 min under a perpendicular magnetic field of 3 T. The resistivity of W and CoFeB layer was determined as 176 $\mu\Omega$cm and 129 $\mu\Omega$cm from the 4 probe analyses, respectively. Fig. 2(b) shows a representative cross-sectional high-resolution transmission electron microscopy (HR-TEM) image of the S-SyAF frame and corresponding energy-dispersive X-ray spectroscopy (EDS) depth profiles. As shown in the right panel of Fig. 2(b), both CoFeB layers (reds) separated by the W layer (magenta) was clearly identified, which indicates that both top and bottom CoFeB layers had easy-axis directions along the film thickness direction [29]. In addition, the FM/HM/FM stacks provided the well-known RKKY interaction between the CoFeB layers. The representative oscillatory behavior of the RKKY interaction versus the W thickness at a fixed FM thickness (1.3 nm in this study) is presented in Supplementary Information 1, where a particular W thickness drives the formation of a clear antiferromagnetic coupling between the top and bottom CoFeB layers, which contributes to an enhancement in the SOT-induced magnetization switching.

## 3. Results and discussion

To evaluate the magnetic and electrical responses of our frame, the sample was patterned into a typical Hall bar shape by utilizing typical photolithography/ion milling processes, as shown in

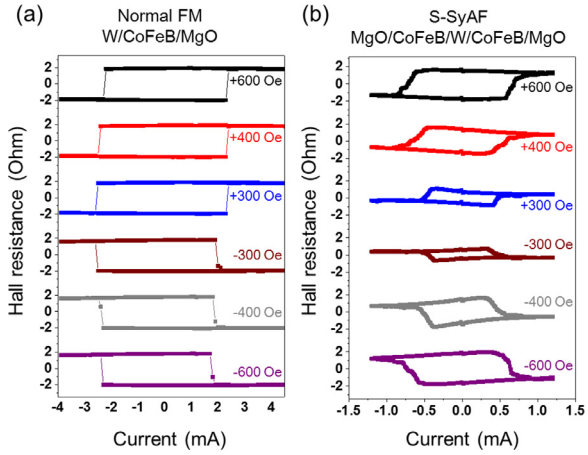


**Fig. 3. Current switching behaviors of the normal HM/FM and S-SyAF frames.** Current-induced magnetization switching of the (a) normal HM/FM and (b) S-SyAF frames under various external magnetic fields ($H_x$), where the critical current necessary for magnetization switching in the S-SyAF frame is considerably smaller than that of the normal HM/FM frame.

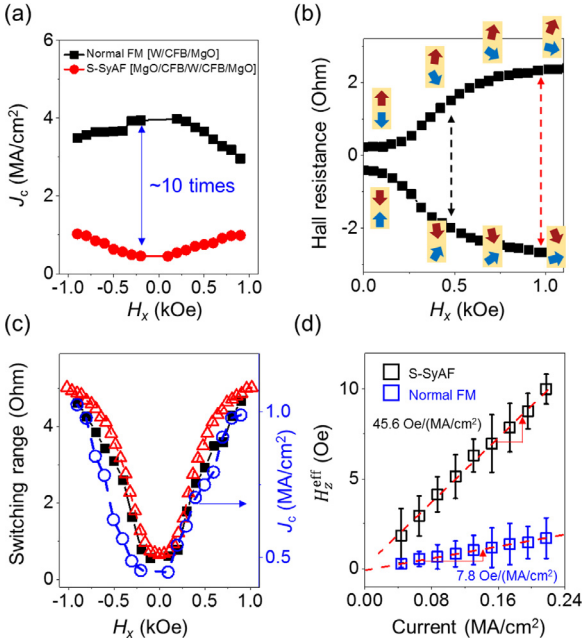


**Fig. 4. Critical current density for magnetization switching and current-induced effective field.** (a) Critical current density versus the variation in the amplitude of the external magnetic field ($H_x$) along the current direction in the normal HM/FM (black) and S-SyAF frames. (b) Enlarged hysteresis loops of S-SyAF under $H_x$ and their magnetization configurations. (c) Difference in Hall resistance between the two switched states versus $H_x$ obtained using the SOT switching curves (black) and hysteresis loops (red), where the blue curve is the enlarged red curve of Fig. 4(a). (d) $Z$ component of the current-induced fields ($\mu_0 H_z^{eff}$) linearly fitted by the red dashed line.

Fig. 2(c). The electrical current ($I_e$) flows along the $x$ axis (the coordinate is defined in Fig. 2(c)). The Hall voltage ($V_H$) is recorded across the Hall cross bar geometry. The Hall resistance ($R_H \equiv V_H/I_e$) is determined mainly with regard to the anomalous Hall effect governed by the $z$ component of the net magnetization [30]. Fig. 2(d) presents the representative magnetic hysteresis loop for the $z$-component magnetization versus the $z$-axis external magnetic field ($H_z$). Both CoFeB layers exhibit antiferromagnetically coupled behaviors at a particular W thickness (2 nm in this study). The specific magnetization configurations of the top and bottom CoFeB layers at certain values of $H_z$ are also described in Fig. 2(d). Note that the figure shows a small gap in the hysteresis loop at zero $H_z$, suggesting a finite difference between the saturation magnetizations of the top and bottom CoFeB layers, although CoFeB layers with identical thicknesses are employed in this study. This is considered to be likely due to differences in dead-layer thicknesses or PMA characteristics between the bottom and top CoFeB layers, which may have originated during the in-situ growth of these layers [31]. Thus, this is denoted as a nearly compensated SyAF frame to distinguish the "up/down" and "down/up" states, and not as a completely compensated antiferromagnetically coupled frame. In addition, the S-SyAF frame exhibits two reversal processes of the top and bottom CoFeB layers upon magnetic field sweeping from the positive to the negative direction. The first reversal exhibits a smooth change, whereas the second reversal is relatively sharp. This behavior can be understood when two FM layers have different PMA characteristics. As mentioned above, the antiferromagnetic RKKY interaction favors an antiparallel alignment, which enables the magnetization before the switching to be tilted such that the parallel component of the CoFeB layers is reduced. However, the tilted magnetizations increase the PMA energy because they have in-plane components. Thus, the competition among the RKKY interactions, PMA, and external magnetic field is attributed to the magnetization switching behaviors. For example, if the increased energy attributed to the PMA in a tilted magnetization state is smaller than the reduced energy induced by the RKKY interaction, a smooth reversal can occur before complete switching.

As depicted above, the passage of a sufficient current through the W layer in S-SyAF leads to "up/down" or "down/up" SOT magnetization switching with respect to the current direction under a fixed $H_x$. Fig. 3 shows the representative switching behaviors of the normal HM/FM and S-SyAF frames. One conventional stack of W (2 nm)/CoFeB (1.3 nm)/MgO (1 nm)/Ta (3 nm) was also fabricated as a normal FM frame for comparison; the normal HM/FM frame is exactly the same as the upper part of S-SyAF. As shown in Fig. 3(a), the normal FM exhibits the typical SOT switching behavior, where the switching direction is reversed when the $H_x$ direction changes due to different symmetry breaking. Moreover, the switching current slightly decreases with the increase in $H_x$ because of the reduction in the effective PMA under $H_x$. However, different magnetization switching behaviors in S-SyAF were observed, as shown in Fig. 3(b). The change in Hall resistance between the two states increases with $H_x$, whereas the normal HM/FM exhibits almost identical Hall resistance changes for various values of $H_x$. Furthermore, the switching current increases with $H_x$, which is the opposite behavior to that of the normal HM/FM frame. The difference in the SOT switching behavior indicates the varied behaviors exhibited by the normal HM/FM and S-SyAF frames, which are described below.

To further validate the SOT switching behavior of S-SyAF, the switching currents were monitored as a function of $H_x$ for the normal HM/FM and S-SyAF, as plotted in Fig. 4(a). Notably, the switching current density (0.45 MA/cm$^2$) necessary for the SOT switching in S-SyAF is almost ten times smaller than that (3.97 MA/cm$^2$) of the normal HM/FM at $H_x$ = 100 Oe. In determining the current density, the sheet resistance of each layer should be considered owing to the appearance of different resistivity, as described above. However, the incorrect factors possibly induced by thickness of dead layer or non-oxidized Ta capping layer can lead to a finite error in calculating the current density. Please note that a variation in current density arising from the different sheet resistance of each layer was about 10 %, as seen in Supplementary Information 3. Therefore, hereafter, we assume the uniform current distribution through the S-SyAF stack for the determination of current densities. This low switching characteristic in the S-SyAF frame is likely to originate from two factors: efficient reduction of magnetization using the antiferromagnetically coupled FM layers and 100% utilization of the spin currents (up and down spin currents) generated by the W layer, as predicted in Fig. 1(c). To quali-

tatively evaluate the above observations, the reduced net magnetization observed in Fig. 2(d) was calculated as follows. The Hall resistances for the "up/up" and "up/down" configurations were 5.18 and 0.35 Ω, respectively. Notably, this state cannot be used to identify which FM layer contributes to a larger saturation magnetization or higher PMA. However, for the analysis, it was assumed that the top CoFeB layer entailed a larger magnetization and PMA. It is worth noting that concerning the opposite case (that is, bottom layer with a higher PMA characteristics), the opposite system is exactly inversion symmetric with the bottom layer with a weaker PMA case, which implies that the switching nature is the same. Therefore, the switching behavior governing the entire S-SyAF system remains unaffected for both cases. $M_s^{\text{top}} + M_s^{\text{bottom}}$ was 5.18 Ω, while $M_s^{\text{top}} - M_s^{\text{bottom}}$ was 0.35 Ω. Therefore, $M_s^{\text{top}}$ of 2.76 Ω and $M_s^{\text{bottom}}$ of 2.41 Ω were estimated. S-SyAF exhibited a net magnetization ($M_s^{\text{top}} - M_s^{\text{bottom}} = 0.35$ Ω) almost ten times smaller than that of the normal HM/FM ($M_{\text{top}} = 2.765$ Ω). Based on Eq. (1), the reduced magnetization significantly contributes to the increase in the SOT efficiency, and thus facilitates an ultralow-current-induced switching event. In the anomalous Hall resistance approach describe above, the size of anomalous Hall resistance cannot reflect the exact value of the magnetization due to the possible variation in Hall resistance contribution created by the presence of non-uniform current distribution or interfacial spin-orbit coupling. But, as depicted in Supplementary Information 3, small contribution for non-uniform current distribution may enable the anomalous Hall resistance–based analyses to be valid in roughly estimating the order of magnitude of change.

To provide insights into the response of the switching currents under $H_x$, the $H_x$-dependent behaviors were evaluated. In the normal HM/FM frame, applying $H_x$ reduces the effective PMA energy according to the $K_{\text{eff}}(1 - \frac{H_x}{H_k})^2$relation. As the effective PMA energy serves as a barrier for magnetization switching between the two states, the application of $H_x$ decreases the switching current density as a function of $H_x^2$ (black dots in Fig. 4(a)). However, in the S-SyAF frame, the net magnetization may be a more dominant parameter. Fig. 4(b) shows representative magnetic hysteresis loops for the $z$ component of the net magnetization as a function of $H_x$, along with specific magnetization configurations corresponding to specific $H_x$ values. Supplementary Information 4 provides the specific magnetization configuration determined from the typical micromagnetic simulation. The bottom CoFeB layer (blue arrows) responds quickly to $H_x$ owing to the weak PMA, which implies that the bottom CoFeB layer was more tilted toward the $x$ axis than the top FM layer. The two CoFeB layers exhibited different magnetization tilting responses, suggesting an increase in the net $z$ component of the total magnetic layers via a reduction in the antiparallel components of each layer with the increase in $H_x$. However, the normal HM/FM exhibits a decrease in the net magnetization with the increase in $H_x$. Although the concept of reduced effective PMA under $H_x$ is still valid in S-SyAF, the variation in the magnetization becomes a dominant parameter because of the considerably higher degree of change. Fig. 4(b) shows the two switched states at two different $H_x$ values, which are marked with black (blue) and red arrows. As $H_x$ tilts the magnetization of each of the top and bottom CoFeB layers, the two stable states for switching also change, along with changes in the switching range, defined as the difference in Hall resistance between the two switched states. As the Hall resistance is determined by the $z$ component of the total system, the angular momentum necessary for switching is proportional to the switching range. This explains the increase in the switching current with $H_x$ for S-SyAF. This behavior is also related to the abnormal change in the switching range as a function of $H_x$. In the normal HM/FM, the switching range was almost identical. However, a large change in the net saturation magnetization of S-SyAF was observed, as described above. Thus, the switching range evaluated using the SOT switching curve in Fig. 4(a) varies as a function of $H_x$ (black dots in Fig. 4(c)). The red triangle curve in Fig. 4(c) represents the difference in the Hall resistance observed in Fig. 4(b), while the blue circle curve represents the enlarged critical current density as a function of $H_x$ for S-SyAF. As the three curves exhibit a substantially narrow and steep parabolic shape, the reduction in the magnetization of S-SyAF is likely associated with the ultralow SOT switching current density. Various switching current densities reported by other groups are presented in Table 1 for comparison. Although the switching current density depends on various parameters, including the HM material, PMA, interface, and FM layer thickness, the S-SyAF exhibited the extremely small SOT switching current characteristics necessary for magnetization switching, in contrast with those of the well-known beta-W/FM-based frame, where the beta-W had the highest SHA. The above analysis is based on the macrospin model. However, the switching mechanism in micron-size devices definitely includes domain wall motion, which needs an initial domain reversal (nucleation) process before it starts. The initial nucleation process corresponds to the macrospin model and the critical switching current is dominantly determined by the nucleation process because the nucleation energy is generally higher than the domain wall motion energy. This is because domain wall motion is a continuous change of magnetization while the nucleation is a discontinuous process. Therefore, we believe that macrospin model is sufficient for explanation of critical switching current density.

To further quantify $\chi$, the $z$ component of the effective SOT field ($H_z^{\text{eff}}$) was also calculated because the switching occurs when the $z$ component of the effective fields exceeds the coercivity field, approximately 25 Oe at zero $H_x$ (Fig. 2(d)). $H_z^{\text{eff}}$ can be obtained as follows. The application of a sufficient $H_x$ that is tilted from the $x$ axis toward the $z$ axis by $\theta_{\text{ext}}$ switches the magnetization state when $H_x \sin\theta_{\text{ext}}$ exceeds the coercivity field. After the current is turned on, the switching $H_x$ changes owing to the presence of $H_z^{\text{eff}}$ via the SOT. The detailed procedure used to obtain $H_z^{\text{eff}}$ is described in Supplementary Information 2. The observed $H_z^{\text{eff}}$ as a function of the current density for the S-SyAF and normal stacks is presented in Fig. 4(d), where the curve slope is associated with the z component of the SOT efficiency ($H_z^{\text{eff}}/J_e$). As seen in this figure, the S-SyAF gives a higher value of 45.6 Oe/(MA/cm$^2$) than the 7.8 Oe/(MA/cm$^2$) of the normal stack. The z component- SOT efficiency of the S-SyAF is about 6 times higher than that of the normal stack. Furthermore, the spin Hall angle of W in the normal stack can be determined from the representative harmonic analysis, where the result was -0.34. Therefore, the spin Hall angle of W in the S-SyAF stack is estimated by employing the z-effective field in the normal and S-SyAF stacks, reduced magnetization, and doubled ferromagnetic layer thickness. The corresponding spin Hall angle of the S-SyAF is -0.36, supporting that an enhancement in SOT efficiency is likely attributed to the reduced magnetization, not the enhanced spin Hall angle. The aforementioned findings can be utilized for the realization of an ultralow current density to overcome the current limitations of spintronic memories, even though more detailed studies are required to attain a theoretical understanding of the underlying nature of these observations.

## 4. Conclusions

We report the ultralow-current-induced SOT switching behaviors of the S-SyAF frame using a current density that is almost ten times smaller than that of the conventional frame. This could be attributed to two advantageous factors, namely, the efficient reduction in the net magnetization of the total magnetic system through the antiferromagnetic RKKY interaction and the possible utilization of both spin currents (100%, up and down) generated by the SHE under the application of electric currents. The systematic ev-

**Table 1**
Summary of SOT switching current densities reported by other groups for various frames and materials.

| Structure (nm) | $J_c$ (MA/cm$^2$) | $H_x$ (Oe) | Ref. |
|---|---|---|---|
| Ta(2)/CoFeB(0.8)/MgO(2) | 6.55 | 400 | [32] |
| Ta(3)/Ru(5)/Ta(4)/CoFeB(0.8)/MgO(1.5) | 2.39 | 12.5 | [33] |
| Pt(5)/Co(0.5)Ta(6) | 1.51 | 200 | [34] |
| Hf(6)/CoFeB(1)/MgO(2) | ~8 | 500 | [35] |
| $\beta$-W(20)/CoFeB(1.1)/MgO(2) | ~17 | 200 | [36] |
| W(5)/CoFeB(1.2)/MgO(1.6) | 10.4 | 200 | [37] |
| W(2)/CoFeB(1.3)/MgO(1) | 3.97 | 200 | This study |
| MgO(1)/CoFeB(1.3)/W(2)/CoFeB(1.3)/MgO(1) | **0.45** | 200 | This study |

idence reveals the potential of suitable FM/HM/FM stacks to suppress magnetization switching currents, thereby revealing a new avenue for high-performance spintronic applications.

## Declaration of Competing Interest

The authors declare that they have no known competing financial interests or personal relationships that could have appeared to influence the work reported in this paper.

## Funding

This study was supported in part by the National Research Foundation of Korea [NRF-2019M3F3A1A03079422, NRF-2016M3A7B4910249] and a National Research Council of Science and Technology grant [No. CAP-16-01-KIST] from the Korean government (MSIP).

## Supplementary materials

Supplementary material associated with this article can be found, in the online version, at doi:10.1016/j.actamat.2021.116708.

## References

[1] I.M. Miron, G. Gaudin, S. Auffret, B. Rodmacq, A. Schuhl, S. Pizzini, J. Vogel, P. Gambardella, Current-driven spin torque induced by the Rashba effect in a ferromagnetic metal layer, Nat. Mater. 9 (3) (2010) 230–234.
[2] I.M. Miron, K. Garello, G. Gaudin, P.J. Zermatten, M.V. Costache, S. Auffret, S. Bandiera, B. Rodmacq, A. Schuhl, P. Gambardella, Perpendicular switching of a single ferromagnetic layer induced by in-plane current injection, Nature 476 (7359) (2011) 189–193.
[3] L. Liu, C.-F. Pai, Y. Li, H.W. Tseng, D.C. Ralph, R.A. Buhrman, Spin–torque switching with the giant spin Hall effect of tantalum, Science 336 (2012) 555–558.
[4] J. Kim, J. Sinha, M. Hayashi, M. Yamanouchi, S. Fukami, T. Suzuki, S. Mitani, H. Ohno, Layer thickness dependence of the current-induced effective field vector in Ta|CoFeB|MgO, Nat. Mater. 12 (3) (2013) 240–245.
[5] G. Yu, P. Upadhyaya, Y. Fan, J.G. Alzate, W. Jiang, K.L. Wong, S. Takei, S.A. Bender, L.T. Chang, Y. Jiang, M. Lang, J. Tang, Y. Wang, Y. Tserkovnyak, P.K. Amiri, K.L. Wang, Switching of perpendicular magnetization by spin–orbit torques in the absence of external magnetic fields, Nat. Nanotechnol. 9 (7) (2014) 548–554.
[6] C.O. Avci, A. Quindeau, C.F. Pai, M. Mann, L. Caretta, A.S. Tang, M.C. Onbasli, C.A. Ross, G.S. Beach, Current-induced switching in a magnetic insulator, Nat. Mater. 16 (3) (2017) 309–314.
[7] W.J. Kong, C.H. Wan, X. Wang, B.S. Tao, L. Huang, C. Fang, C.Y. Guo, Y. Guang, M. Irfan, X.F. Han, Spin–orbit torque switching in a T-type magnetic configuration with current orthogonal to easy axes, Nat. Commun. 10 (1) (2019) 233.
[8] S. Bhatti, R. Sbiaa, A. Hirohata, H. Ohno, S. Fukami, S.N. Piramanayagam, Spintronics based random access memory: a review, Mater, Today 20 (9) (2017) 530–548.
[9] J. Ryu, S. Lee, K.J. Lee, B.G. Park, Current–induced spin–orbit torques for spintronic applications, Adv. Mater. 32 (35) (2020) 1907148.
[10] W. Zhang, W. Han, X. Jiang, S.-H. Yang, S.S.P. Parkin, Role of transparency of platinum–ferromagnet interfaces in determining the intrinsic magnitude of the spin Hall effect, Nat. Phys. 11 (6) (2015) 496–502.
[11] K.U. Demasius, T. Phung, W. Zhang, B.P. Hughes, S.H. Yang, A. Kellock, W. Han, A. Pushp, S.S.P. Parkin, Enhanced spin–orbit torques by oxygen incorporation in tungsten films, Nat. Commun. 7 (2016) 10644.
[12] M. DC, R. Grassi, J.-Y. Chen, M. Jamali, D. Reifsnyder Hickey, D. Zhang, Z. Zhao, H. Li, P. Quarterman, Y. Lv, M. Li, A. Manchon, K.A. Mkhoyan, T. Low, J.-P. Wang, Room-temperature high spin–orbit torque due to quantum confinement in sputtered $Bi_xSe_{(1-x)}$ films, Nat. Mater. 17 (9) (2018) 800–807.
[13] L. Zhu, D.C. Ralph, R.A. Buhrman, Highly efficient spin–current generation by the spin Hall effect in $Au_{1-x}Pt_x$, Phys. Rev. Appl. 10 (3) (2018) 031001.
[14] P.X. Zhang, L.Y. Liao, G.Y. Shi, R.Q. Zhang, H.Q. Wu, Y.Y. Wang, F. Pan, C. Song, Spin-orbit torque in a completely compensated synthetic antiferromagnet, Physical Review B 97 (21) (2018) 214403.
[15] C. Bi, H. Almasi, K. Price, T. Newhouse-Illige, M. Xu, S.R. Allen, X. Fan, W. Wang, Anomalous spin-orbit torque switching in synthetic antiferromagnets, Physical Review B 95 (10) (2017) 104434.
[16] X. Zhao, W. Liu, S. Li, T. Wang, L. Liu, Y. Song, S. Ma, X. Zhao, Z. Zhang, Asymmetric current–driven switching of synthetic antiferromagnets with Pt insert layers, Nanoscale 10 (16) (2018) 7612–7618.
[17] E.A. Tremsina, N. Roschewsky, S. Salahuddin, Micromagnetic analysis and optimization of spin-orbit torque switching processes in synthetic antiferromagnets, Journal of Applied Physics 126 (16) (2019) 163905.
[18] J. Finley, L. Liu, Spin-Orbit-Torque Efficiency in Compensated Ferrimagnetic Cobalt-Terbium Alloys, Physical Review Applied 6 (5) (2016) 054001.
[19] R. Mishra, J. Yu, X. Qiu, M. Motapothula, T. Venkatesan, H. Yang, Anomalous Current-Induced Spin Torques in Ferrimagnets near Compensation, Physical Review Letters 118 (16) (2017) 167201.
[20] K. Cai, Z. Zhu, J.M. Lee, R. Mishra, L. Ren, S.D. Pollard, P. He, G. Liang, K.L. Teo, H. Yang, Ultrafast and energy-efficient spin–orbit torque switching in compensated ferrimagnets, Nat. Electron. 3 (1) (2020) 37–42.
[21] C.-F. Pai, M. Mann, A.J. Tan, G.S.D. Beach, Determination of spin torque efficiencies in heterostructures with perpendicular magnetic anisotropy, Phys. Rev. B 93 (14) (2016) 144409.
[22] C.-F. Pai, Y. Ou, L.H. Vilela-Leão, D.C. Ralph, R.A. Buhrman, Dependence of the efficiency of spin Hall torque on the transparency of Pt/ferromagnetic layer interfaces, Phys. Rev. B. 92 (6) (2015) 064426.
[23] S.H. Yang, K.S. Ryu, S. Parkin, Domain-wall velocities of up to 750 m $s^{-1}$ driven by exchange-coupling torque in synthetic antiferromagnets, Nat. Nanotechnol. 10 (3) (2015) 221–226.
[24] Y.C. Lau, D. Betto, K. Rode, J.M. Coey, P. Stamenov, Spin-orbit torque switching without an external field using interlayer exchange coupling, Nat. Nanotechnol. 11 (9) (2016) 758–762.
[25] S.C. Baek, V.P. Amin, Y.W. Oh, G. Go, S.J. Lee, G.H. Lee, K.J. Kim, M.D. Stiles, B.G. Park, K.J. Lee, Spin currents and spin-orbit torques in ferromagnetic trilayers, Nat. Mater. 17 (6) (2018) 509–513.
[26] M.A. Ruderman, C. Kittel, Indirect exchange coupling of nuclear magnetic moments by conduction electrons, Phys. Rev. 96 (1) (1954) 99–102.
[27] T. Kasuya, A theory of metallic ferro- and antiferromagnetism on Zener's model, Prog. Theor. Phys. 16 (1) (1956) 45–57.
[28] K. Yosida, Magnetic properties of Cu–Mn alloys, Phys. Rev. 106 (5) (1957) 893–898.
[29] S. Ikeda, K. Miura, H. Yamamoto, K. Mizunuma, H.D. Gan, M. Endo, S. Kanai, J. Hayakawa, F. Matsukura, H. Ohno, A perpendicular-anisotropy CoFeB–MgO magnetic tunnel junction, Nat. Mater. 9 (9) (2010) 721–724.
[30] N. Nagaosa, J. Sinova, S. Onoda, A.H. MacDonald, N.P. Ong, Anomalous Hall effect, Rev. Mod. Phys. 82 (2) (2010) 1539–1592.
[31] S. Yang, J. Lee, G. An, J. Kim, W. Chung, J. Hong, Ta thickness-dependent perpendicular magnetic anisotropy features in Ta/CoFeB/MgO/W free layer stacks, Thin Solid Films 587 (2015) 39–42.
[32] X. Qiu, P. Deorani, K. Narayanapillai, K.S. Lee, K.J. Lee, H.W. Lee, H. Yang, Angular and temperature dependence of current induced spin-orbit effective fields in Ta/CoFeB/MgO nanowires, Sci. Rep. 4 (2014) 4491.
[33] M. Bapna, B. Parks, S.D. Oberdick, H. Almasi, W. Wang, S.A. Majetich, Spin–orbit–torque switching in 20-nm perpendicular magnetic tunnel junctions, Phys. Rev. Appl. 10 (2) (2018) 024013.
[34] J. Yun, D. Li, B. Cui, X. Guo, K. Wu, X. Zhang, Y. Wang, Y. Zuo, L. Xi, Spin–orbit torque induced magnetization switching in Pt/Co/Ta structures with perpendicular magnetic anisotropy, J. Phys. D Appl. Phys. 50 (39) (2017) 395001.
[35] R. Ramaswamy, X. Qiu, T. Dutta, S.D. Pollard, H. Yang, Hf thickness dependence of spin–orbit torques in Hf/CoFeB/MgO heterostructures, Appl. Phys. Lett. 108 (20) (2016) 202406.
[36] C. Zhang, S. Fukami, K. Watanabe, A. Ohkawara, S. DuttaGupta, H. Sato, F. Matsukura, H. Ohno, Critical role of W deposition condition on spin–orbit torque induced magnetization switching in nanoscale W/CoFeB/MgO, Appl. Phys. Lett. 109 (19) (2016) 192405.
[37] S. Cho, S.C. Baek, K.D. Lee, Y. Jo, B.G. Park, Large spin Hall magnetoresistance and its correlation to the spin–orbit torque in W/CoFeB/MgO structures, Sci. Rep. 5 (2015) 14668.